Available online at www.sciencedirect.com

ScienceDirect

IFAC PapersOnline CONFERENCE PAPER ARCHIVE

IFAC PapersOnLine 56-2 (2023) 8221–8226

Consideration of Tissue Deformation through an Electrode Displacement in a Monopolar Coagulation Model ⋆

Christoph Busch * **Stefan J. Rupitsch** ** **Knut Moeller** *

* *Institute of Technical Medicine (ITeM), Furtwangen University, 78054 Villingen-Schwenningen, Germany (e-mail: bc@hs-furtwangen.de).*

** *Department of Microsystems Engineering, University of Freiburg, 79110 Freiburg, Germany (e-mail: stefan.rupitsch@imtek.uni-freiburg.de)*

Abstract: In today's surgery, high-frequency electrical currents are often used to achieve various effects, one important being the heating of tissue to stop bleeding. However, the physical processes of tissue heating are complex and not fully understood. This complicates medical device approval with the settings used for such applications. Therefore, a simulation approach can help provide evidence. In this contribution, we present a modification of a model already presented and described in a previous investigation. By incorporating continuum mechanics into our model, we were able to simulate the deformation of the tissue due to electrode displacement. The resulting deformed configuration was then used to simulate Joule heating by applying a constant direct current voltage and to analyze the effect of varying the electrode displacement depth on the heat distribution result. Our results show that the contact area of the electrode to the tissue plays a crucial role in heating the tissue. This is because the tissue heats up more slowly with a large contact area than with a small one, resulting in significantly greater heat propagation to deeper tissue regions.

Keywords: FEM simulation, HF modeling, hyperelastic material, incompressible tissue, monopolar coagulation

1. INTRODUCTION

High-frequency (HF) surgery is a common surgical method that has been used for many years. It uses HF alternating current to induce hemostasis. This involves the heating of biological tissue through which the current flows. The heating at the cellular level is due to Joule's heating. Despite decades of use, evidence of the efficacy and safety of HF applications for medical approval is still lacking. Modeling approaches can economically support medical approval processes, but the models used must reliably represent reality. Therefore, it is necessary to investigate how reality can be adequately represented using a modeling approach. For this purpose, multi-physical processes occurring in the application must be identified and understood.

Different mathematical approaches are already available and can be used as a basis for our needs. In our first survey, we built a monopolar coagulation finite element (FE) model of liver tissue based on Pennes (1948) bioheat equation with adaptions from Yang et al. (2007) and Chen et al. (2013) as described in Busch et al. (2022). There, we investigated the temperature distribution in biological tissue with changing initial values of temperature-dependent tissue parameters. A limitation of the presented model was that no tissue deformation due to the contact pressure of the HF electrode on the tissue was considered. The FE model described in this contribution will take this into account and overcome this limitation. Different displacement depths of the electrode perpendicular to the biological tissue surface are analyzed. The analysis includes the influence of different electrode-tissue contact surfaces on the temperature distribution in the tissue.

⋆ This work was partially supported by the German Federal Ministry of Research and Education (BMBF) under grant number 13FH5I07IA (CoHMed/SmartMed A).

2. MATERIALS AND METHODS

Based on our previous work (Busch et al., 2022), we modified the 2 dimensional (2D) axisymmetric monopolar coagulation FE model by adding continuum mechanics, i.e., a mechanical problem. In this approach, we split our simulation into two study steps. In the first step, we solved the mechanical problem, whereupon in the second step the results from the first step were used to solve the electrically thermally coupled problem. In the end, the simulation reveals the temperature distribution in the biological tissue. For both simulation steps, we used the COMSOL Multiphysics® (2021) software and a workstation with an AMD Ryzen 7 3700x 8-Core processor and 64 GB of working memory.

2.1 Mechanical Problem

When modeling a continuum mechanics approach for biological tissue, the hyperelasticity of the tissue has to be considered (Wex et al., 2015). However, before we elaborate on the hyperelastic material model in more detail, some general definitions are given first. The tissue in its initial stress-free position at t_0 (undeformed or reference configuration) is an open bounded domain defined as $\Omega_0 \subset \mathbb{R}^2$ with boundary $\partial\Omega_0$, whereas Ω is defined as the tissue domain in the current deformed configuration at t with boundary $\partial\Omega$. Therefore, the motion of the tissue can be described by the mapping function χ for $\chi : \Omega_0 \rightarrow \Omega$.

10.1016/j.ifacol.2023.10.1004

χ maps a particle defined through its position vector $\mathbf{X} \in \Omega_0$ at t_0 to the particles position $\mathbf{x} \in \Omega$ at t through $\mathbf{x} = \chi(\mathbf{X},t)$ (see Fig. 1). The movement of the particle can also be described by the displacement vector $\mathbf{u}(\mathbf{X}, t)$ with $\mathbf{x} = \mathbf{X} + \mathbf{u}(\mathbf{X}, t)$. By taking the gradient of the mapping function, we get the deformation gradient tensor $\mathbf{F} = \partial\mathbf{x}/\partial\mathbf{X} = \nabla\mathbf{x} = \nabla\chi(\mathbf{X},t)$. Whereas the Jacobian of the deformation gradient tensor describes the volume ratio or, in other words, the volume change from Ω_0 to Ω and is defined through $J = V/V_0 = \det(\mathbf{F})$, where V_0 and V are the initial volume and the current volume, respectively. If $J < 1$, domain compression takes place, whereas $J > 1$ describes expansion. If J is equal to 1, no volume change occurs, i.e., an isochoric process is present. Furthermore, the deformation gradient tensor can be used to define the right Cauchy-Green deformation tensor by $\mathbf{C} = \mathbf{F}^{\mathrm{T}}\mathbf{F}$, where $^{\mathrm{T}}$ denotes the transpose.

When modeling biological tissue for structural analysis as hyperelastic material, different hyperelastic material models can be used (Wex et al., 2015; Holzapfel et al., 2000), resulting in different characteristic strain energy density functions W_{s}. We assumed that the tissue is isotropic, whereby the W_{s} only depends on the invariants of the right Cauchy-Green deformation tensor. For our model, we used the Neo Hookean hyperelastic material model, which is defined by

$$W_{\mathrm{s}} = \frac{\lambda}{2}[\ln(J)]^2 - \mu\ln(J) + \frac{\mu}{2}(I_1 - 3), \tag{1}$$

where λ and μ are the first and second Lamé parameters respectively, J is the volume ratio, and I_1 is the first invariant (trace) of the right Cauchy-Green deformation tensor defined by $I_1 = \mathrm{tr}(\mathbf{C})$.

We further assume in our model that biological tissue is incompressible so that $J = 1$ holds. So (1) can be simplified to

$$W_{\mathrm{s}} = \frac{\mu}{2}(I_1 - 3). \tag{2}$$

The second Lamé parameter in (2) is defined by

$$\mu = \frac{1}{2} \cdot \frac{1}{1+\nu} \cdot E, \tag{3}$$

where ν is Poisson's ratio and E is Young's modulus. The values used for Poisson's ratio and Young's modulus of the electrode (stainless steel) and incompressible liver tissue are shown in table 1.

Now that our hyperelastic material model for the tissue is defined, the second Piola-Kirchhoff stress can be calculated as

$$\mathbf{S} = 2\frac{\partial W_{\mathrm{s}}}{\partial \mathbf{C}}, \tag{4}$$

which gives the material stress in the reference configuration.

2.2 Thermal and electrical coupled problem

Once the mechanical problem was solved by a rigid body displacement of the Ø 4 mm ball electrode, the result was used to calculate the heat distribution induced by Joule heating in the tissue. The model utilized, which combines the thermally and electrically coupled problem in a partial differential equation, is the bioheat equation from Pennes (1948) and is defined by

$$\rho c_{\mathrm{eff}}(T)\frac{\partial T}{\partial t} = \nabla \cdot k(T)\nabla T + \mathbf{J}\cdot\mathbf{E} - \omega_{\mathrm{b}} c_{\mathrm{b}} \rho_{\mathrm{b}} (T - T_{\mathrm{b}}), \tag{5}$$

where ρ is the tissue density, ρ_{b} is the blood density, $c_{\mathrm{eff}}(T)$ is the temperature-dependent effective heat capacity, T and t are the temperature and the time respectively, T_{b} is the blood temperature, $k(T)$ is the temperature-dependent thermal conductivity, $\mathbf{J}$ is the current density, $\mathbf{E}$ is the electrical field intensity, ω_{b} is the effective capillary blood perfusion parameter and c_{b} is the blood heat capacity. The current density is defined by Ohm's law $\mathbf{J} = \sigma(T)\mathbf{E}$, where $\sigma(T)$ is the temperature-dependent electrical conductivity and the electrical field intensity is given by the negative gradient of the applied voltage V, $\mathbf{E} = -\nabla V$. To keep the model simple, we have assumed a quasi-static approach to solving the electrical problem using Laplace's equation, which is defined by

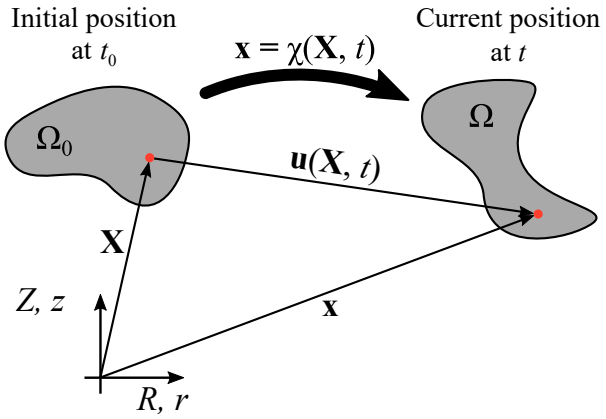

Fig. 1. Schematic representation of a body transformation including displacement, rotation, and deformation from the initial body position at time t_0 to the transformed current position at time t under the representation of used vector definitions.

$$\nabla \cdot \sigma(T)\nabla V = 0. \tag{6}$$

For determining $k(T)$ we applied the linear approximation

$$k(T) = k_{\mathrm{ref}} + k_1(T - T_{\mathrm{ref}}), \tag{7}$$

where k_1 is a control coefficient, k_{ref} is the initial thermal conductivity at the reference temperature $T_{\mathrm{ref}} = 25$ °C and T is the current temperature.

For the temperature-dependent electrical conductivity $\sigma(T)$, we followed Chen et al. (2013) and used a piecewise function defined by

$$\sigma(T) = \begin{cases} \sigma_{\mathrm{ref}}[1 + 0.02(T - T_{\mathrm{ref}})] & T < 100\ ^{\circ}\mathrm{C} \\ 0.01\ \mathrm{S/m} & T \geq 100\ ^{\circ}\mathrm{C} \end{cases}, \tag{8}$$

where T is again the current temperature, σ_{ref} is the initial electrical conductivity at the reference temperature $T_{\mathrm{ref}} = 25$ °C. As in Busch et al. (2022), we applied the continuous first derivative for smoothing $\sigma(T)$ at the transition point of $T = 100$ °C. The multiplication of the temperature-dependent tissue water content $W(T)$ with $\sigma(T)$ for considering the loss of water due to desiccation was omitted because the water loss is already considered in $\sigma(T)$ due to the decrease of σ to 0.01 S/m at $T \geq 100$ °C.

The temperature-dependent effective heat capacity $c_{\mathrm{eff}}(T)$ as well as the temperature-dependent tissue water content $W(T)$ were modeled identically to our previous study and is explained in Busch et al. (2022). As initial tissue water content, we used 80 %. All model parameters used are shown in table 1.

Table 1. Model material parameters

Material parameter		Value	Unit	Source
Liver tissue				
- Poisson's ratio	ν_t	0.5		
- Young's modulus	E_t	1.98	kPa	Umale et al. (2013)
- density	ρ	1079	kg/m^3	IT'IS Foundation (2022)
- thermal conductivity	k_{ref}	0.52	$W/(m \cdot K)$	IT'IS Foundation (2022)
- electrical conductivity	σ_{ref}	0.13	S/m	IT'IS Foundation (2022)
- control coefficient	k_1	0.001161	$W/(m \cdot K \cdot °C)$	Valvano et al. (1985)
- water content	W_{ref}	0.8		
Stainless steel (ball electrode)				
- Poisson's ratio	ν_{el}	0.29		Ledbetter et al. (1980)
- Young's modulus	E_{el}	200	GPa	Ledbetter et al. (1980)
Blood				
- density	ρ_b	1050	kg/m^3	IT'IS Foundation (2022)
- heat capacity	c_b	3617	$J/(kg \cdot K)$	IT'IS Foundation (2022)
- temperature	T_b	37	°C	
- capillary perfusion parameter	ω_b	0.0064	$1/s$	Trujillo and Berjano (2013)

2.3 Model setup, boundary conditions, and solver settings

As already mentioned, the FE model utilized for these simulations is based on the model described in Busch et al. (2022), but with slight modifications to integrate the mechanical problem. Therefore, the geometry of the Ø 4 mm ball electrode and the liver tissue (2.5×2.5 cm) is identical to our previous investigation. The main difference is that the electrode is not already inserted into the tissue block, but the two surfaces of the electrode and the tissue are just touching. The arrangement of the electrode and the tissue used for the first study step, as well as the displacement field $\mathbf{u}$ of the electrode, which is perpendicular to the tissue surface, are illustrated in Fig. 2.

To generate the mesh of the electrode and of the tissue, the meshing generator of COMSOL Multiphysics® (2021) was used. The tissue block was built as a mapped mesh with a maximum quadrilateral element size of 0.2 mm, whereas the electrode was meshed with triangles and a maximum element size of 0.694 mm. In total, the FE model consists of 16082 elements, of which 15876 are quadrilateral and 206 triangular.

For the initial conditions of the mechanical problem, no displacement field and no contact pressure were set. When considering the boundary conditions, we defined the upper and right tissue surfaces, as well as the electrode surface, as free-movable surfaces. In contrast, the bottom surface of the tissue was fixed so that $\mathbf{u} = 0$ applies to this boundary. In order to perform the contact simulation, we had to define source and destination boundaries for the contact pair (electrode to tissue). For this purpose, the surface of the ball electrode was set as the source boundary and the upper tissue surface as the destination boundary. The contact friction was neglected in this simulation. Additionally, we selected the augmented Lagrangian method with an automatic penalty factor as convergence control for computing the contact.

The mechanical problem was solved with a stationary study, where the vertical displacement u_z of the electrode was swept from 0 to 3 mm in 0.05 mm steps. To save computation time and due to expected large elastic deformations of the tissue, an incremental solution update was used by adding the block Elastic Predeformation in COMSOL. By storing the deformation history with the used displacement field $\mathbf{u}$, the total deformation is calculated from incremental steps (Structural Mechanics Module User's Guide, 2019). The COMSOL Multiphysics® (2021) linear direct solver MUMPS was used to solve the stationary study. The computation time of the first study step was 4 h 46 min and 6 s.

The electrically thermally coupled problem was solved by a time-dependent study with a simulation time of 10 s and a step size of 0.05 s. The boundary conditions of these two physics were set as described in Busch et al. (2022). In this second simulation step, we used the contact simulation results of the previously solved mechanical problem. Only the results for the electrode displacements u_z with 0.5 mm, 1.0 mm, 1.5 mm, 2.0 mm, 2.5 mm, and 3.0 mm were used for the time-dependent study. As linear direct solver of the second study step, we used the PARDISO solver (COMSOL Multiphysics®, 2021). The computation time of the second study step was 27 min and 41 s.

3. RESULTS

Fig. 3 shows the simulation results of both study steps, whereby Fig. 3A) to Fig. 3F) illustrates the energy stored in the hyperelastic tissue due to the electrode displacement via the strain energy density from the first study step from 0.5 to 3.0 mm in 0.5 mm displacement steps. It can be seen that the larger the electrode displacement, the greater the strain energy density in the tissue. For a linear displacement of the electrode in the z-direction, as shown in Fig. 3A) to Fig. 3F), a nonlinearity of the resulting strain energy density can be recognized. The total strain energy density $W_{s,tot}$ is obtained by taking the volume integral of the tissue area. Whereby $W_{s,tot}$ increases from Fig. 3A)

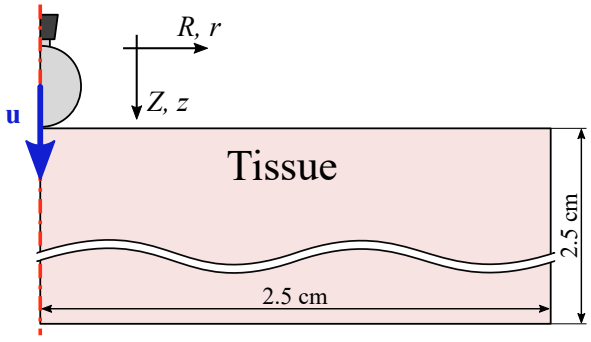

Fig. 2. Schematic of the 2D axisymmetric monopolar coagulation model consisting of a 2.5 cm quadradic tissue block with a Ø 4 mm ball electrode used as reference configuration for the first study step - solving the mechanical problem.

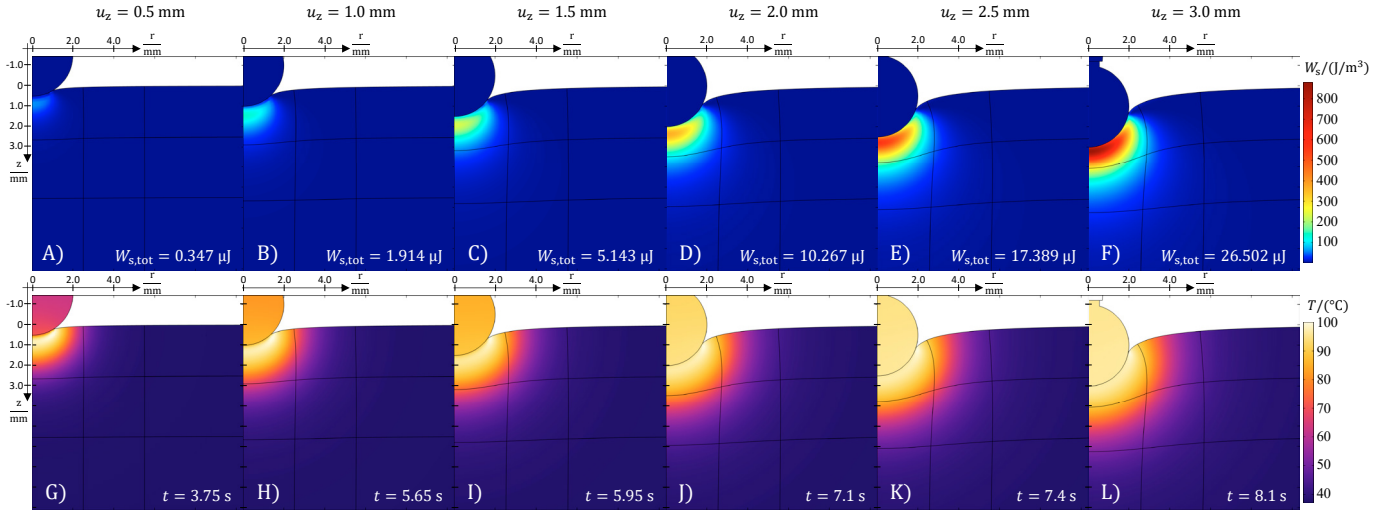

Fig. 3. Simulation results from the first and second study steps. A) to F) shows the deformed tissue with the stored strain energy density $(\mathrm{J/m^3})$ resulting from the six different electrode displacement depths A) 0.5 mm, B) 1.0 mm, C) 1.5 mm, D) 2.0 mm, E) 2.5 mm and F) 3.0 mm of the first study step. Additionally, $W_{s,tot}$, the total stored strain energy $(\mu\mathrm{J})$, was calculated by taking the volume integral of W_s of the tissue area. In G) to L), the temperature distributions $(^\circ\mathrm{C})$ of the second study step corresponding to the displacement depths from A) to F) are shown. Here H) to L) shows the temperature distribution at the time when the boiling point of water is reached.

to 3B) about 1.567 μJ, from Fig. 3B) to 3C) about 3.229 μJ, from Fig. 3C) to 3D) about 5.124 μJ, from Fig. 3D) to 3E) about 7.122 μJ, and from Fig. 3E) to 3F) about 9.113 μJ. The nonlinear increase in $W_{s,tot}$ resulting from the linear electrode displacements is also shown in graph A) of Fig. 4. There, the simulation results are represented by the circular data points. The dashed line in the diagram illustrates a smoothing spline curve fit of the simulation data. This nonlinear behavior is expected when using a hyperelastic formulation due to the nonlinear relation between strain and stress.

The maximum contact pressures $p_{0,max}$ resulting from the electrode displacements were also determined and are shown in graph B) of Fig. 4. Again, the simulation results of $p_{0,max}$ are illustrated in the circular data points, whereas the smoothing spline curve fit of $p_{0,max}$ is represented by the dashed line. If one considers the contact pressure to be applied for the selected electrode displacements, the characteristic of biological tissue as soft tissue becomes clear. Already 0.21295 $\mathrm{N/cm^2}$ is sufficient to result in a displacement of 3 mm, which brings almost half of the ball electrode surface into tissue contact (see Fig. 3F). Furthermore, the results in graph B) of Fig. 4 show that the maximum contact pressure does not increase linearly with u_z. The reason is that the linear electrode displacement leads to a nonlinear increase in the electrode-tissue contact surface.

A substantial part of this contribution addressed the implementation of a hyperelastic material model into an existing coagulation model. It served to obtain a more representative deformation of the biological tissue at the contact surface to the ball electrode. Based thereon, we obtained the final results of interest, which are the heat distributions in Fig. 3G) to Fig. 3L) representing the actual impact of the electrical current on the tissue. The figures show the temperature distribution in the tissue at the time when the boiling point of water is reached. It can be seen that the larger the contact area between the electrode and the tissue at a constant applied voltage, the longer it takes to reach 100 °C in the tissue.

The results in Fig. 3G) illustrate that the tissue near the contact surface (at about 0.125 to 0.25 mm depth below the contact surface) reaches 100 °C first. At this point, the electrode itself has only reached about 60 to 70 °C. This leads to a thin layer of tissue at the contact surface, from about 0.065 to 0.125 mm depth, where a negative temperature gradient to the electrode can be observed. This indicates that the electrode cools the tissue contact area as long as its temperature is lower than that of the tissue. This is most likely due to the much higher electrical conductivity and thus, lower resistivity of the stainless steel. Wherefore, Joule heating is more intense in the tissue than in the electrode. In Fig. 3H), where the contact area is greater than in Fig. 3G) and the time until the tissue reaches 100 °C increases by 1.9 s, the negative gradient from the 100 °C tissue spot toward the electrode decreases. This is due to the further increase in the electrode temperature to about 80 °C.

4. DISCUSSION

The electrode temperature increases the longer the tissue is exposed to the current and the larger the contact surface becomes. Since in our modeled case, the thermal and electrical conductivity of stainless steel is larger than those of the biological tissue, the increase in electrode temperature from Fig. 3G) to Fig. 3L) is expected to be primarily due to heat transfer between the tissue and the electrode. Thus, this depends on both, the electrode contact area and the application time. Furthermore, a larger contact area also means the contact resistivity between the electrode and the tissue becomes lower. Consequently, the current density at the contact surface decreases, resulting in slower tissue heating until 100 °C is reached. Slow tissue heating leads to better heat distribution not only in the tissue but also in the electrode. Therefore, the cooling effect of the electrode is almost undetectable at the contact surface. This can already

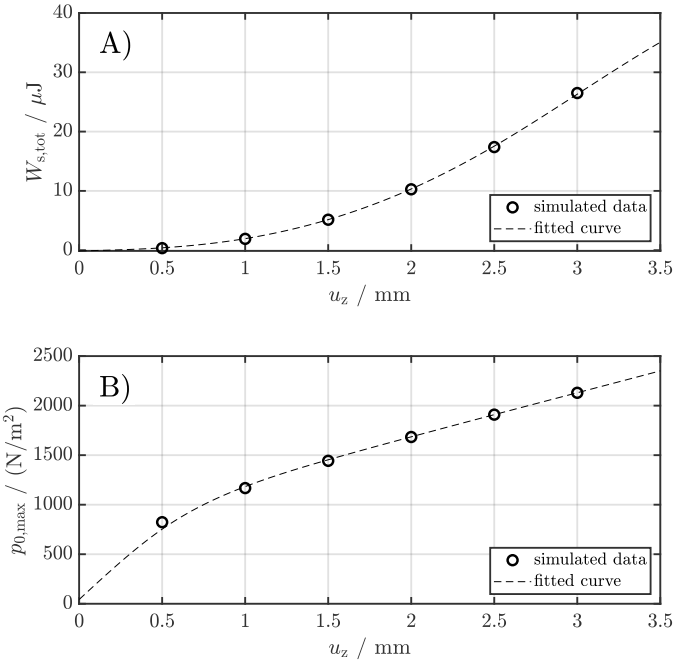

Fig. 4. The simulated total strain energy density $W_{s,tot}$ in μJ and the maximum contact pressure $p_{0,max}$ in N/m^2 are shown in circular data points over the electrode displacement depth u_z in mm in graphs A) and B), respectively. In both cases, a smoothing spline curve fit was performed, which is represented by the dashed line.

be discerned at an electrode displacement of $u_z = 2.0$ mm in Fig. 3J). In Fig. 3L) the cooling effect is no longer visible.

The results indicate that the depth of tissue heat distribution is related to the current density, which in turn, is associated with the electrode contact surface. If the contact surface becomes larger, whereas the applied voltage is constant, it takes longer to reach 100 °C in the tissue, and therefore, the temperature has more time to distribute in deeper tissue regions. If deep coagulation is needed, this can be achieved by reducing the HF generator's output power or by just applying a higher electrode pressure to the tissue. (Whereby in this context, deep coagulation is understood as a deep temperature distribution.) In both cases, slower heating occurs due to the lower current density and longer current application time.

In contrast, a smaller contact surface (caused by less pressure) leads to faster and superficial tissue heating at the same constant voltage. The faster heating leads to a highly resistive tissue region near the electrode contact surface when 100 °C is reached. As soon as the tissue has exceeded the boiling point, it is assumed that the water in the tissue has desiccated, resulting in a high resistivity in this area. It is then difficult for the current to flow through this tissue area because the electrical conductivity of the tissue without water is very low. The highly resistive tissue area reduces the current flow and tissue heating in deeper regions. It has to be noted that the implemented model and the temperature-dependent tissue parameters considered in it are valid only below the boiling point of water. Therefore, validation tests are required to investigate the assumptions made for this application and confirm their validity.

These findings show that the pressure of the electrode on the tissue is one of the decisive factors for the desired tissue heating effect. It can be seen that with a constant applied voltage, the energy input, and thus the heat generation in the tissue, is highly dependent on the contact area of the HF instrument to the tissue. Likewise, it can be deduced that the choice of the electrode can significantly influence heat distribution through its size and geometry. That is, by its contact area with the tissue.

5. CONCLUSIONS

By adding continuum mechanics and tissue deformation to our simulation model, we are one step closer to the goal of representing multiple physical processes in biological tissue. However, there are still some unknown processes as well as physical limitations in the current model that have not yet been considered and require further investigation and analysis.

We have shown that the contact area between the electrode and the tissue plays an important role in Joule heating and heat distribution in the tissue when the applied direct current voltage is kept constant. This leads to a decrease in the current density at the contact area and thus slower heating of the tissue when the contact area is increased. By adapting the applied voltage as a function of tissue resistivity, it would be possible to take the contact area into account, since the contact area is directly proportional to the contact resistance (electrode to tissue). Also, no alternating HF current has been considered in the model so far. Adding this to the model might make it possible to model different heating effects due to modulation of the alternating HF current. One effect of HF current-induced heating that has been frequently mentioned is tissue desiccation. Although the evaporation of water in the tissue is already taken into account in the temperature-dependent tissue parameters, shrinkage of the drying tissue has not yet been integrated.

These simulations provide a basis to better understand physical processes during tissue coagulation. However, a quantitative evaluation of our simulation results might be possible only after the validation of the model. Therefore, it is necessary to clarify how appropriate validation can be implemented, performed, and analyzed.

REFERENCES

Busch, C., Rupitsch, S.J., and Moeller, K. (2022). Influence of temperature-dependent tissue parameters on monopolar coagulation model. *Current Directions in Biomedical Engineering*, 8(2), 466–469. doi:10.1515/cdbme-2022-1119. Publisher: De Gruyter.

Chen, R.K., Chastagner, M.W., Dodde, R.E., and Shih, A.J. (2013). Electrosurgical vessel sealing tissue temperature: experimental measurement and finite element modeling. *IEEE transactions on bio-medical engineering*, 60(2), 453–460. doi:10.1109/TBME.2012.2228265.

COMSOL Multiphysics® (2021). v. 6.0. *COMSOL AB, Stockholm, Sweden*. URL `www.comsol.com`.

Holzapfel, G.A., Gasser, T.C., and Ogden, R.W. (2000). A New Constitutive Framework for Arterial Wall Mechanics and a Comparative Study of Material Models. *Journal of elasticity and the physical science of solids*, 61(1), 1–48. doi:10.1023/A:1010835316564.

IT'IS Foundation (2022). Database of tissue properties. URL `https://itis.swiss/virtual-population/tissue-properties/database/`.

Ledbetter, H.M., Frederick, N.V., and Austin, M.W. (1980). Elastic-constant variability in stainless-steel 304. *Journal*

of Applied Physics, 51(1), 305–309. doi:10.1063/1.327371. Publisher: American Institute of Physics.

Pennes, H.H. (1948). Analysis of Tissue and Arterial Blood Temperatures in the Resting Human Forearm. *Journal of Applied Physiology*, 1(2), 93–122. doi:10.1152/jappl.1948.1.2.93. Publisher: American Physiological Society.

Structural Mechanics Module User's Guide (2019). *COMSOL Multiphysics® v. 6.0, COMSOL AB, Stockholm, Sweden*, 380–382. URL `https://doc.comsol.com/5.5/doc/com.comsol.help.sme/StructuralMechanicsModuleUsersGuide.pdf`.

Trujillo, M. and Berjano, E. (2013). Review of the mathematical functions used to model the temperature dependence of electrical and thermal conductivities of biological tissue in radiofrequency ablation. *International Journal of Hyperthermia*, 29(6), 590–597. doi:10.3109/02656736.2013.807438.

Umale, S., Deck, C., Bourdet, N., Dhumane, P., Soler, L., Marescaux, J., and Willinger, R. (2013). Experimental mechanical characterization of abdominal organs: liver, kidney & spleen. *Journal of the Mechanical Behavior of Biomedical Materials*, 17, 22–33. doi:10.1016/j.jmbbm.2012.07.010.

Valvano, J.W., Cochran, J.R., and Diller, K.R. (1985). Thermal conductivity and diffusivity of biomaterials measured with self-heated thermistors. *International Journal of Thermophysics*, 6(3), 301–311. doi:10.1007/BF00522151.

Wex, C., Arndt, S., Stoll, A., Bruns, C., and Kupriyanova, Y. (2015). Isotropic incompressible hyperelastic models for modelling the mechanical behaviour of biological tissues: A review. *Biomedizinische Technik. Biomedical engineering*, 60. doi:10.1515/bmt-2014-0146.

Yang, D., Converse, M.C., Mahvi, D.M., and Webster, J.G. (2007). Expanding the bioheat equation to include tissue internal water evaporation during heating. *IEEE transactions on bio-medical engineering*, 54(8), 1382–1388. doi:10.1109/TBME.2007.890740.